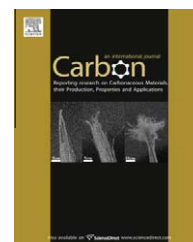
available at www.sciencedirect.comjournal homepage: www.elsevier.com/locate/carbon

Graphene-modified carbon fiber mats used to improve the activity and stability of Pt catalyst for methanol electrochemical oxidation

Yunzhen Chang, Gaoyi Han ^{*}, Miaoyu Li, Fei Gao

Institute of Molecular Science, Key Laboratory of Chemical Biology and Molecular Engineering of Education Ministry, Shanxi University, Taiyuan 030006, China

ARTICLE INFO

Article history:

Received 21 April 2011

Accepted 30 June 2011

Available online 22 July 2011

ABSTRACT

Graphene-modified carbon fiber mats (GCFMs) with high conductivity of about 65 S cm^{-1} and good flexibility have been fabricated by thermally treating electrospun polyacrylonitrile fibers decorated with graphene oxide. Pt particles were then deposited on the GCFM by using formaldehyde vapor as a reducer to react with $\text{H}_2\text{PtCl}_6 \cdot 6\text{H}_2\text{O}$ adsorbed on the GCFM. The obtained electro-catalytic electrodes were characterized and evaluated. The results show that the Pt catalyst loaded on GCFM exhibits high electro-catalytic activity, good tolerance towards reaction intermediates and unusually high stability towards methanol electrochemical oxidation because the special structure of GCFM can stabilize the Pt particles, and that the charge transfer resistance between the methanol and the catalytic electrode is as small as $15.7 \Omega\text{cm}^2$. An electrochemical catalyst with high activity and stability can be developed by using GCFM as a supporting material.

© 2011 Elsevier Ltd. All rights reserved.

1. Introduction

Direct methanol fuel cells (DMFCs) which convert chemical energy of methanol directly into electrical energy through catalytic reaction are very useful working systems adopted by the electric vehicles and electronic portable devices due to their high efficiency and environmentally-benign property [1–6]. At present, Pt and its alloy are usually used as the cathode and anode catalysts for the oxygen reduction and methanol oxidation in DMFCs, respectively. However, it is necessary to improve the performances of Pt-based catalysts for methanol electro-oxidation because of such barriers as low methanol oxidation kinetics, the aggregation and poisoning of the catalyst exhibited during the commercialization of DMFCs. Thus, it is significant to improve the activity of Pt-based catalysts used in methanol electro-oxidation [7].

It has been proved that the performances of catalysts are closely associated with not only the size, morphology and

distribution of the particles of catalysts but also the nature of the supporting materials. Tests of durability have indicated that conventional carbon black supports undergo morphological changes and induce aggregation of catalysts during the extended use [8]. Therefore, special attention has been paid to use the various carbon materials including mesocarbon microbeads [9], ordered mesocarbon microbeads [10,11], activated carbon fibers (CFs) [12,13], carbon nanotubes (CNTs) [14–16] and other carbonaceous materials [17–19] as supports for catalysts. Recently, the conductive fiber mats fabricated by electrospinning present potential applications in DMFCs because their large cumulate pores among the continuous nanofibers are favorable for the diffusion of the reagent and the flow of liquid and gas [13,20]. More attention has still focused on the improvement of the initial activity of the catalysts in most researches although the stability, especially the long-term stability of catalysts is the same important as its activity in methanol electrochemical oxidation [21].

^{*} Corresponding author. Fax: +86 351 7016358.

E-mail address: han_gaoyis@sxu.edu.cn (G. Han).

0008-6223/\$ - see front matter © 2011 Elsevier Ltd. All rights reserved.

doi:10.1016/j.carbon.2011.06.099

Graphene, a newly found carbon material, constructed by a single layer of carbon atom possessing large surface area as well as excellent electronic conductivity, large thermal conductivity [22–24], has stimulated great interest and intense studies in recent years because of its various potential applications in many technological fields [25–28]. Till now, different techniques including micromechanical exfoliation, epitaxial growth and chemical vapor deposition have been developed for producing graphene. Chemically converted graphene (CCG) synthesized by using graphite, graphene oxide (GO) or other graphite derivatives as starting materials has been found to be a useful component in various composites [29,30] and can improve the properties of the composites. Recently, it is found that CCG can improve the activity of Pt catalyst towards methanol oxidation dramatically in DMFCs [31–34]. However, the surface area of the CCG will be decreased strikingly when the separated graphene sheets aggregate together through the force of van der Waals and the interaction of π - π although the separated graphene sheets exhibit large surface area, this will influence the utility and performances of the catalysts supported on them. It is expected that the performances including the activity and stability of Pt catalyst will be improved when the hybrid carbon materials prepared from one- and two-dimensional materials of carbon are used as a support considering that the surface of the fibers will be modified by CCG and the CCG sheets will be separated by the nanofibers when the structures of one-dimensional nanofibers prepared by electrospinning and the two-dimensional CCG are combined.

In present work, GO is used as decorator to modify the surface of electrospun polyacrylonitrile (PAN) fibers firstly by simply filtering the GO solution through the fiber mats of PAN. After thermally-treated, graphene-modified carbon fiber mats (GCFMs) are obtained and used as the supports to load Pt particles prepared by reacting formaldehyde vapor with $\text{H}_2\text{PtCl}_6 \cdot 6\text{H}_2\text{O}$ adsorbed on them. The fabricated catalytic electrode is expected to exhibit high activity and long-term stability.

2. Experimental

2.1. Chemicals and materials

Natural graphite powder (NGP, 325 mesh) was purchased from Tianjin Guangfu Research Institute. PAN and Nafion solution (5%) were obtained from Aldrich and the commercial Pt/C (40%) was bought from Johnson Matthey Corp. All other chemicals employed in this study were of analytical grade. The fiber mats of PAN were prepared according to the previously reported method [20]. The GO was prepared by oxidizing the NGP according to the method reported in literature [35]. To make the size of the GO smaller, the obtained GO was treated by mixed acids according to the improved method for treating CNTs [36]. Briefly, GO (400 mg) was added into 20.0 mL mixture of H_2SO_4 and HNO_3 (3:1 by volume), then the mixture was poured into cold water after ultrasonic treating for 16 h. The resulted precipitate was collected and washed with large amount of water, and followed by dialysis for one week to remove the remaining acid and ions. Finally, the collected gel-like GO was dried under vacuum condition in the presence of P_2O_5 .

2.2. Preparation of GCFMs

The diluted dispersion of GO was prepared by dispersing 4.5 mg GO into 200 mL water under ultrasonic bath for 60 min. The electrospun fiber mat of PAN was placed on the filter membrane carefully and the GO dispersion was added into the cullender cautiously and filtered through the mat slowly after filtering 100 mL water. The fiber mat of PAN decorated with GO was then obtained when the dispersion of GO filtered through the mat completely, and then the hybrid mats were transferred into a muffle furnace for oxidative stabilization at 280 °C. Finally, the GCFMs were obtained after the oxidative stabilized hybrid fiber mats were heated at 600 °C for 30 min firstly and then the temperature was increased to 1200 °C and kept for 1 h under high-purity argon atmosphere. The resulted GCFMs (thickness: 50 μm) were cut by a razor blade into rectangular strips with an approximate size of 10 \times 2 mm and used as electrodes directly. For comparison carbon fiber mats (CFMs) were also prepared according to the method reported in literature [20].

2.3. Preparation of catalytic electrodes

The Pt particles were synthesized by reacting $\text{H}_2\text{PtCl}_6 \cdot 6\text{H}_2\text{O}$ adsorbed on GCFMs with formaldehyde vapor. The typical procedure was described as the follows: firstly, tetrahydrofuran (60 μL) was mixed with 0.19 mol L^{-1} $\text{H}_2\text{PtCl}_6 \cdot 6\text{H}_2\text{O}$ aqueous solution (20 μL), secondly, a certain amount of the mixture was adsorbed onto GCFM, subsequently the films of GCFMs containing Pt precursor were placed into a small glass tube which would be placed into 20 mL Teflon-sealed autoclave containing 1.0 mL formaldehyde (37%) aqueous solution and 100 μL CH_3OH after the solvent was volatilized in the air (25 °C), and then the Teflon-sealed autoclave was heated in an oven and kept at 125 °C for 3 h. After cooling, the catalytic electrodes were washed by ethanol and water thoroughly and dried in air, and denoted as Pt-GCFM. By comparison, the catalytic electrodes denoted as Pt-CFM were fabricated by depositing Pt particles on CFMs in the similar procedure. The electrodes assigned as Pt/GCFM were also fabricated by loading the commercial Pt/C on the GCFM through transferring 6.4 μL of the ultrasonic-treated mixture of Pt/C catalyst (5.0 mg), water (1.25 mL) and Nafion solution (0.25 mL) onto the GCFM. The content of Pt in all the electrodes was kept about 0.21 mg cm^{-2} . And the geometric surface area of the electrodes was guaranteed to be about 0.04 cm^2 .

2.4. Characterization and measurement

Scanning electron micrographs (SEM) and transmission electron micrographs (TEM) images were observed by employing a JEOL-JSM-6701 field-emission microscope operating at an accelerating voltage of 10 kV and a JEM-1011 transmission electron microscope operating at the accelerating voltage of 80 kV, respectively. Raman spectra were recorded on a JobinYvon Lab RAMHR800 microscopic confocal Raman spectrometer by employing a laser of 514 nm as incident light. The time for each measurement was 30 s and the spectra were recorded by accumulating the measurement for three times. X-ray diffraction (XRD) patterns were recorded on a

Bruker D8 Advance X-ray diffractometer with Cu K_{α} radiation and graphite monochromator, at the scan speed of 5°min^{-1} with a step size of 0.02° . The content of Pt was determined by an IRIS Advantage inductively coupled plasma atomic emission spectroscopy system. The electrical conductivity was measured by using the four-probe method, and electrochemical measurements were carried out on a CHI 660C electrochemistry workstation at 25°C . The electrolyte was $0.5\text{ mol L}^{-1}\text{ H}_2\text{SO}_4 + 1.0\text{ mol L}^{-1}\text{ CH}_3\text{OH}$ aqueous solution, the Pt-CFM, Pt-GCFM and Pt/C-GCFM electrodes, a Pt plate and saturated calomel electrode (SCE) were used as working, counter and reference electrode, respectively. Electrochemical impedance spectroscopy (EIS) was carried out in the frequency ranging from 100,000 to 0.1 Hz with amplitude of 5 mV, and ZView-2 fitting program was used to analyze the impedance parameters. High-purity N_2 was used to deaerate the solutions and maintained above the electrolyte solution during measurements.

3. Results and discussion

3.1. Characteristic of the fiber mats

It can be seen clearly from Fig. 1 that the surface structure of the CFs has changed obviously after they are modified by CCG through comparing the typical morphologies of the GCFMs with that of CFMs. Formed by CFs bearing relatively smooth surface and an even diameter distribution ($\sim 150\text{ nm}$), the CFM possesses many cumulate gaps formed by the carbon fibers (Fig. 1A). However, the surface of the CFs in the GCFM has become quite coarse, and the diameter of the fibers becomes slightly larger too. Furthermore, some gaps between the fibers

are found to be covered by some CCG sheets (Fig. 1B). From the TEM image inserted in Fig. 1B, it can be seen that the CFs are coated closely by the CCG sheets whose surface is crinkly, which makes the surface of the CFs rough. From the Raman spectra of the CFM and GCFM, two typical peaks which are corresponding to the defect/disorder-induced vibrational mode (D band) and the E_{2g} vibrational mode which is activated for sp^2 hybridized carbon-based material (G band) are observed at about 1342 and 1588 cm^{-1} , respectively (Fig. 1C). The value of D/G (the area ratio of D to G band) can be used to denote the relative content of graphited carbon in the carbonaceous materials. It is surprising to find that the D/G value in the Raman spectrum of the GCFM is larger than that of CFM, which indicates that the GCFM possesses more modes of defect/disorder-induced vibration because of the increment of the sp^3 carbon atoms' variety and the structural damage on the ordered structure of graphene deposited on the surface of CFs. That is due to the fact that sp^2 carbon network has been broken into nano-scale oxidized domain during the process that GO is fabricated [37,38]. As shown in Fig. 1D, it is clear that the strips of GCFM exhibit good flexibility, and that the strip with a length of 35 mm and a width of 2 mm can be bent easily. The electrical conductivities are measured by convenient four-probe method, and it is found that the GCFM exhibits (65 S cm^{-1}) higher conductivity than CFM (45 S cm^{-1}).

The double-layer capacities of the GCFM and CFM are also determined in $1.0\text{ mol L}^{-1}\text{ KCl}$ aqueous solution (Fig. 2) in order to illustrate the changes of the surface area. It can be found that the cyclic voltammetry (CV) curves are rectangular-like with the almost symmetric I-E responses for the both electrodes, which are corresponding to the rapid current

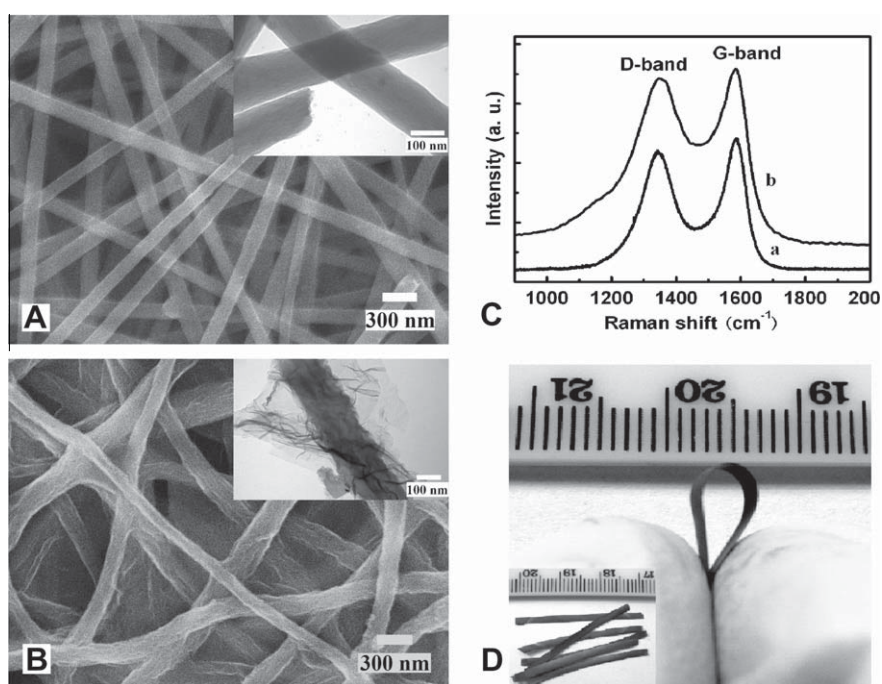


Fig. 1 – (A) SEM images of CFM (insertion: magnified SEM image), (B) SEM of GCFM (insertion: TEM image of GCFM), (C) Raman spectra of the CFM (a) and GCFM (b) as prepared and (D) the GCFM strip under bent situation (insertion: the photograph of the GCFM strips with the size of $35 \times 2 \times 0.05\text{ mm}$).

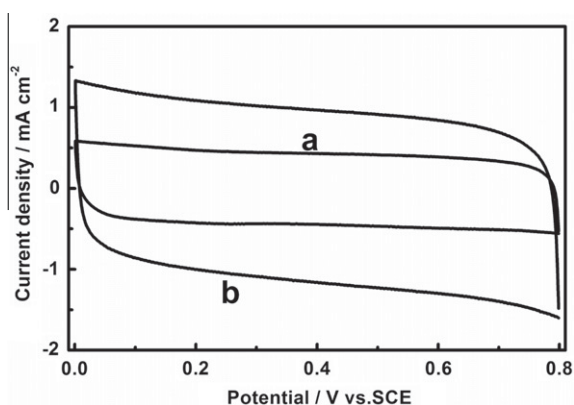


Fig. 2 – CV curves in 1.0 mol L^{-1} KCl aqueous solution for (a) CFM and (b) GCFM electrodes with a scan rate of 300.0 mV s^{-1} .

response on voltage reversal at each end potential and accord with the ideal capacitive behavior. The double-layer capacity of GCFM (3.75 mF cm^{-2}) is about $2.57\times$ as high as that of CFM (1.46 mF cm^{-2}) based on the geometrical area, indicating that the modified CCG can increase the surface of CFM. The above results reveal that the CCG can not only reform the surface structure of carbon nanofibers but also improve the flexibility of the CFM and the electrical conductivity, which will cause the GCFM to be suitable as supporting materials for electrochemical catalysts.

3.2. Characteristics of the mats loaded with Pt particles

The noble metallic particles of Pt are loaded on the fiber mats through reacting Pt precursor with formaldehyde vapor. From the SEM image shown in Fig. 3A, it can be seen that the Pt particles are deposited on the surface of the fibers and the CCG in GCFM, the size of Pt particles is very small and relatively uniform, and what is more, relatively more Pt particles are dispersed in the intersectional region among the fibers. From the TEM image (Fig. 3B), it is corroborated clearly that the Pt particles disperse not only on the surface of CF but also on the CCG, the size of the Pt particles ranges from 3 to 7 nm; furthermore, it can be also found that the density of the Pt particles is high on the fringe of the fiber close to the CCG sheets. In contrast, the Pt particles with the relatively large size are deposited on the surface of CFs uniformly in CFM (Fig. 3C), from the inserted TEM image, it can be seen that the size of the Pt particles deposited on CFM ranges from 5 to 10 nm. In the XRD patterns (Fig. 3D), the diffraction peak located at about 24.9° is assigned to the diffraction of C (2 0 0) plane, while the peaks at 39.8 , 46.4 and 67.6° are corresponding to the diffraction of Pt (1 1 1), (2 0 0) and (2 2 0) plane. According to the Scherrer formula ($d = 0.89\lambda/B\cos\theta$), the average diameter of Pt particles is calculated to be about 3.7, 5.2 and 7.3 nm for Pt/C, Pt-GCFM and Pt-CFM electrodes, respectively, which is consistent with the results obtained from TEM images.

3.3. Performances of the catalytic electrodes

The activity of the catalytic electrodes towards the methanol oxidation is evaluated by using the CV method in the

electrolyte of $1.0 \text{ mol L}^{-1} \text{ CH}_3\text{OH} + 0.5 \text{ mol L}^{-1} \text{ H}_2\text{SO}_4$ at a potential scan rate of 50 mV s^{-1} . It can be seen clearly from Fig. 4A that the anodic current density on Pt-GCFM electrode in the positively going scan (I_f) increases with the increase of scan potential, and that at 0.78 V the peak current density reaches to 101.0 mA cm^{-2} ($468 \text{ mA mg}^{-1} \text{ Pt}$) (Fig. 4A-c) which is significantly larger than 84.0 mA cm^{-2} ($400 \text{ mA mg}^{-1} \text{ Pt}$) on Pt-CFM electrode at 0.75 V (Fig. 4A-b) and 41.2 mA cm^{-2} ($194 \text{ mA mg}^{-1} \text{ Pt}$) on commercial Pt/C-GCFM electrode at 0.68 V (Fig. 4A-a) although the CV curve of GCFM does not show significant redox activity (Fig. 4A-d). At the same time, the other anodic peak (I_b) observed in the reverse scan can be attributed to the removal of the incompletely oxidized carbonaceous species formed in the positively going scan whose relative amount can be evaluated by using the I_f/I_b value. It is interesting to find that the I_f/I_b value is about 1.09 for methanol oxidation on the Pt-GCFM electrode, which is higher than that on Pt-CFM electrode (0.98) and commercial catalyst Pt/C loaded on GCFM (0.93), indicating that more effective oxidation of methanol occurs on Pt-GCFM electrode during the forward potential scan and that less poisoning species can form compared with Pt-CFM and Pt/C-GCFM electrodes [20,34].

It can be found from Fig. 4B that the current density of methanol oxidation on Pt-GCFM electrode is much higher than that on the Pt-CFM and Pt/C-GCFM electrodes when the potential is larger than 0.22 V based on the plots of the potential dependence on the steady-state current density recorded at 100 s. The ratios of the current density on Pt-GCFM versus that acquired on Pt-CFM or Pt/C-GCFM, reach to 344% for Pt/C-GCFM and 307% for Pt-CFM at 0.35 V , and 244% for Pt/C-GCFM and 190% for Pt-CFM at 0.45 V , respectively. This result indicates that the reaction of methanol oxidation occurs on the Pt-GCFM electrode easier than on Pt-CFM and Pt/C-GCFM electrodes.

Electrochemically active surface areas (ECSAs) of Pt nanoparticles on various electrodes are also measured in deaerated $0.5 \text{ mol L}^{-1} \text{ H}_2\text{SO}_4$ aqueous solution by using CV method at sweep rate of 50 mV s^{-1} , as shown in Fig. 5. It is clear that all electrodes exhibit the features of hydrogen adsorption-desorption within the region of -0.24 – 0.1 V . Using the value of 0.21 mC cm^{-2} for a clean planar Pt electrode [39], the ECSAs of the electrodes are calculated by integrating the area under the hydrogen desorption wave and found to be 44.5, 34.8 and $32.8 \text{ m}^2 \text{ g}^{-1}$ for Pt nanoparticles on Pt/C-GCFM, Pt-GCFM and Pt-CFM electrodes, respectively. The results are consistent with the size of the Pt particles obtained by TEM image and XRD patterns.

In order to investigate the sole effect of the supports, the peak current densities of the methanol oxidation normalized by the ECSA of Pt nanoparticles (j_{ECSA}) are obtained by using the equation according the method reported previously [40]:

$$j_{\text{ECSA}} = \frac{j_{\text{MPt}}}{\text{ECSA}_{\text{Pt}}} \quad (1)$$

where j_{MPt} is the peak current density of methanol oxidation normalized by the mass of Pt. The values of j_{ECSA} are calculated to be 0.44, 1.34 and 1.22 mA cm^{-2} for Pt/C-GCFM, Pt-GCFM and Pt-CFM electrodes, respectively. The results demonstrate that the activity of Pt particles towards methanol oxidation can also be influenced by the supporting

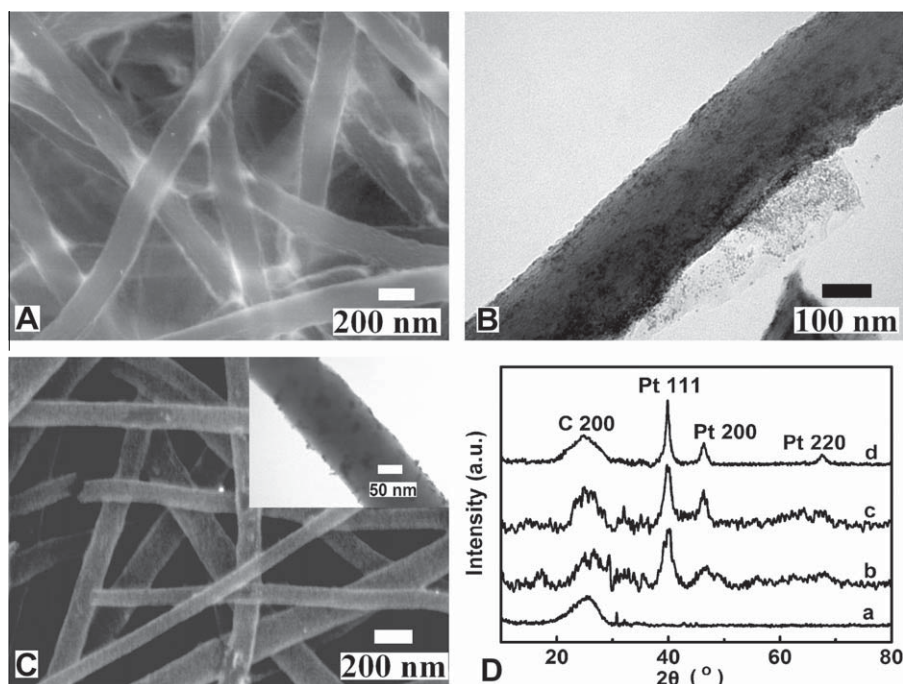


Fig. 3 – SEM images of the Pt-GCFM (A) and Pt-CFM (C) electrodes recorded by combining the back-scattered electron and secondary electron images, the insertion in (C) is the TEM image of Pt-CFM electrode, the TEM image of the Pt-GCFM electrode (B), and (D) the XRD patterns of GCFM (a), Pt/C-GCFM (b), Pt-GCFM (c) and Pt-CFM (d) electrodes.

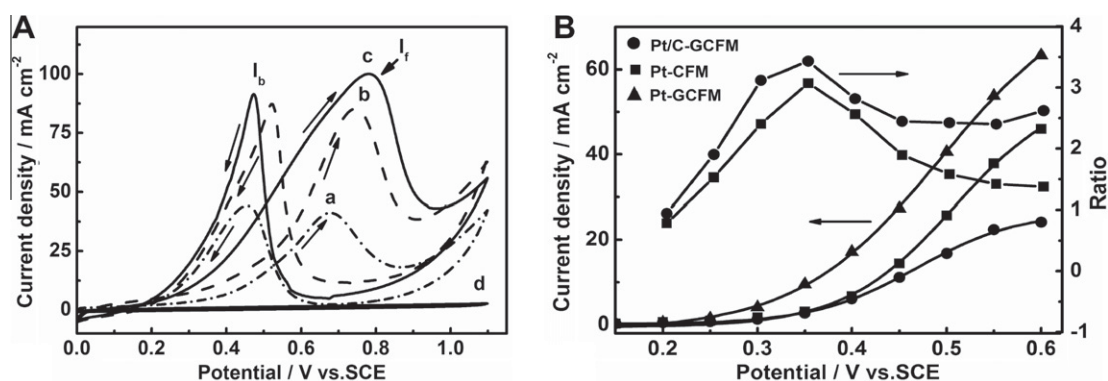


Fig. 4 – (A) CV curves for methanol oxidation on (a) Pt/C-GCFM, (b) Pt-CFM, (c) Pt-GCFM and (d) GCFM electrodes at scan rate of 50 mV s^{-1} , (B) Potential-dependent steady-state current densities (left, recorded at 100 s) of the methanol oxidation on the catalytic electrodes, and the ratios (right) between the current density obtained on Pt-GCFM with that on Pt-CFM and Pt/C-GCFM electrodes, respectively. Electrolyte: N_2 saturated $0.5 \text{ mol L}^{-1} \text{ H}_2\text{SO}_4 + 1.0 \text{ mol L}^{-1} \text{ CH}_3\text{OH}$ aqueous solution.

materials, and that the CCG modified on the carbon fibers can improve the activity of Pt nanoparticles.

In order to get more information about the reactive process and the kinetics of methanol oxidation, EIS from which the charge transfer resistance (R_{ct}) can be obtained according to the relationship between ac impedance and the frequency of ac sources [41] are measured. From the complex plots measured at 0.35 V (Fig. 6A), it is found that the semicircle or arc at low frequency appears in all the complex plots and varies with the difference of electrodes. It is interesting to find that the impedance data plotted in the complex plane extend into the fourth quadrant for Pt-GCFM electrode, while the data for Pt-CFM and Pt/C-GCFM electrodes remain in the first

quadrant, except that the curvature for Pt-CFM electrode is larger than that for Pt/C-GCFM electrode. The R_{ct} value is evaluated as $15.7 \Omega \text{ cm}^2$ for Pt-GCFM electrode by using the equivalent circuit inserted in Fig. 6A, which is much smaller than $28.1 \Omega \text{ cm}^2$ for Pt-CFM electrode and $41.6 \Omega \text{ cm}^2$ for Pt/C-GCFM electrode. Such result shows clearly that a rather quick charge transfer rate has realized on Pt-GCFM electrode during methanol electro-oxidation.

In practical application, both the activity and the long-term stability of the catalysts are important. So the stabilities of the Pt-GCFM, Pt-CFM and Pt/C-GCFM electrodes have also been determined by chronoamperometric technique at a technical interesting potential in fuel cell application

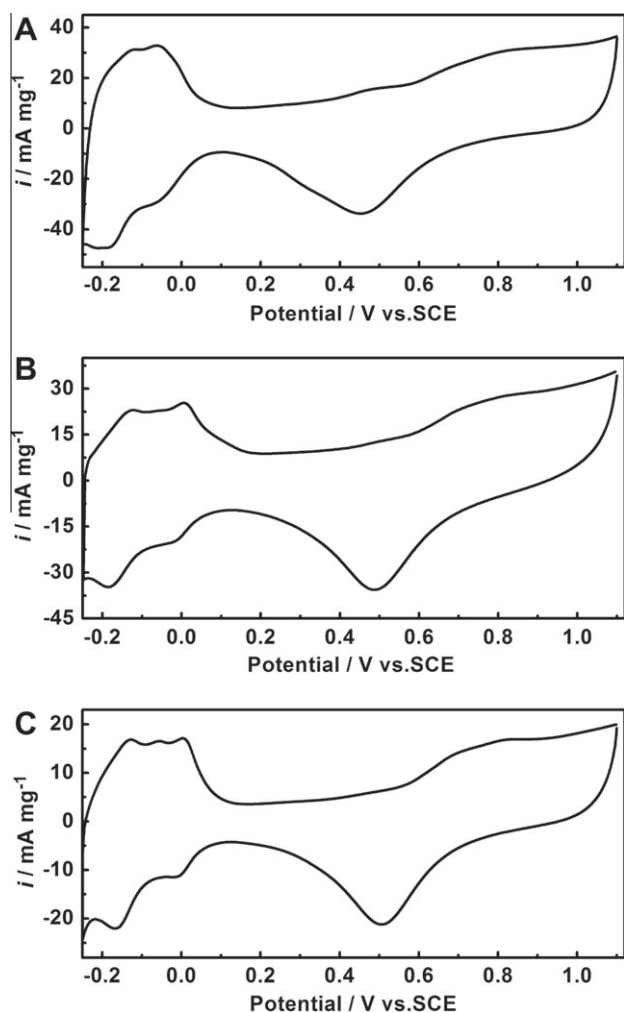


Fig. 5 – The CV curves of Pt/C-GCFM (A), Pt-GCFM (B) and Pt-CFM (C) electrodes in N_2 saturated $0.5 \text{ mol L}^{-1} \text{ H}_2\text{SO}_4$ solution at a potential scan rate of 50 mV s^{-1} .

(0.45 V) for $10,000 \text{ s}$ (Fig. 6B). It can be seen obviously that the current densities of methanol oxidation present continuous decay with the increment of time after reaching their maxima

of 32.2 , 22.9 and 19.7 mA cm^{-2} on Pt-GCFM, Pt-CFM and Pt/C-GCFM electrodes, respectively. Moreover, the decay of the current density on Pt-GCFM electrode exhibits a more gently decreasing trend than the other electrodes. After a polarization for 1000 s , the current densities decrease to 24.4 , 11.1 and 5.87 mA cm^{-2} on Pt-GCFM, Pt-CFM and Pt/C-GCFM electrodes, respectively. Finally, the current densities retain 12.1 , 2.7 and 0.97 mA cm^{-2} , which hold the maxima of 37.8% , 11.8% and 4.9% on Pt-GCFM, Pt-CFM and Pt/C-GCFM electrodes after a polarization of $10,000 \text{ s}$, respectively. Namely, the reserved current density on Pt-GCFM electrode is about $12.9\times$ as high as that on Pt/C-GCFM electrode and about $4.4\times$ as that on Pt-CFM electrode after steady-state polarization of $10,000 \text{ s}$. From the results shown in Figs. 4 and 6, it can be found that the Pt-GCFM electrode exhibits excellent electro-catalytic activity and long-term stability toward methanol oxidation, indicating that the Pt-GCFM electrode possesses good tolerance towards reaction intermediates and favors long-term application as the anode in DMFCs.

3.4. The structural changes after stability test

Fig. 7 shows the changes of microstructure on the electrodes after stability test. It can be seen that the density of Pt particles on graphene becomes higher than that before stability test and the size of the catalyst particles increases slightly although the distribution of the Pt particles still keeps relatively uniform (Fig. 7A). Furthermore, from the inserted SEM image (the white color represents Pt), it is interesting to find that most of Pt particles have transferred to the intersectional region among the fibers where more CCG exists comparing with the electrode as prepared (Fig. 2A). The size of Pt particles dispersed on the surface of CFs in CFM increases obviously, for example, it has enlarged from 7.3 to about 10 nm (Fig. 7B) after stability test. From the inserted SEM image, one can also find that many particles with the size of about 50 nm have dispersed on the surface of fibers, which is quite different from the observation on Pt-GCFM electrodes where the Pt particles are still relatively uniform.

The main causes that lead to the changes may be the fact that the surface of CFs has been modified by CCG which

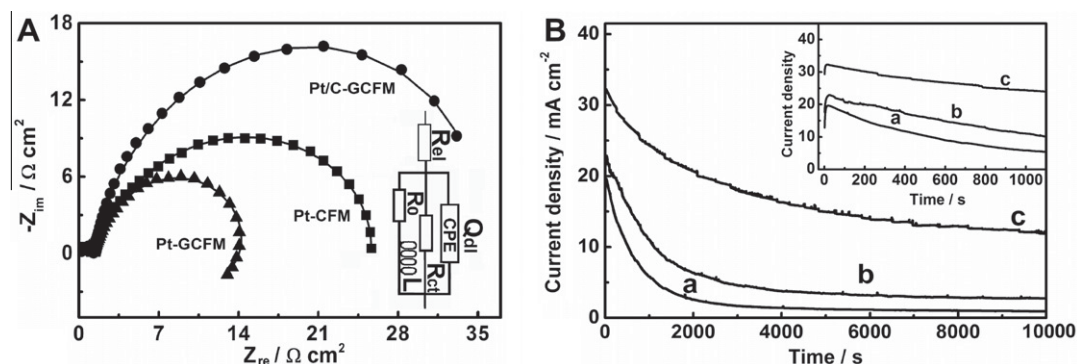


Fig. 6 – (A) Complex plane plots of the impedance of the Pt/C-GCFM, Pt-CFM and Pt-GCFM electrodes at potential of 0.35 V (insertion: the equivalent circuit can simulate the data), (B) Long-term stability test: chronoamperometric curves of methanol oxidation on Pt/C-GCFM (a), Pt-CFM (b) and Pt-GCFM (c) electrodes a constant potential of 0.45 V (insertion: the chronoamperometric curves before 1500 s). Electrolyte: N_2 saturated $0.5 \text{ mol L}^{-1} \text{ H}_2\text{SO}_4 + 1.0 \text{ mol L}^{-1} \text{ CH}_3\text{OH}$ aqueous solution.

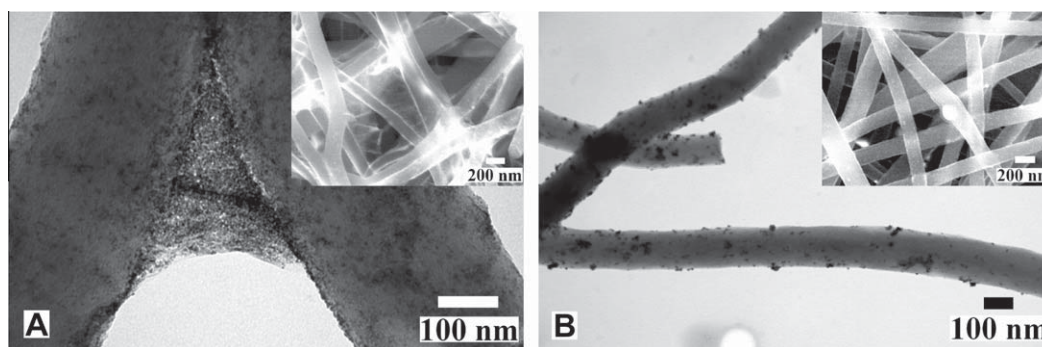


Fig. 7 – TEM images of Pt-GCFM (A) and Pt-CFM (B) electrodes after the stability test of 10,000 s. SEM images inserted are recorded by combining the back-scattered and secondary electron images.

prevents the Pt particles from agglomeration. It is that the new surface of fibers has now become coarser, and exhibits larger specific surface area than the old surface without CCG. On the other hand, the introduced CCG exhibits many defect-disorder domains which are favorable for the dispersion of catalysts, which has been pointed out that the surface of graphene under the condition of tension can stabilize the Pt particles [42]. So the high activity and long-term stability of Pt particles may come from the above-mentioned factors.

4. Conclusions

Graphene-modified carbon fiber mats have been fabricated by combining the electrospinning, surface decoration and thermal treatment. The surface of the carbon nanofibers becomes rough after they are modified by CCG and at the same time the CCG sheets are separated by the fibers. The material used as the support improves both the activity and long-term stability of the Pt catalyst towards methanol oxidation dramatically, which indicates that it can be developed as an excellent supporting material for electrochemical catalysts.

Acknowledgements

The authors thank the National Natural Science Foundation of China (Grant No. 21073115 and 20604014), the Program for New Century Excellent Talents in University (NCET-10-0926) of China and the Program for the Top Young and Middle-aged Innovative Talents of Higher Learning Institutions of Shanxi province (TYMIT and TYAL).

Appendix A. Supplementary data

Supplementary data associated with this article can be found, in the online version, at [doi:10.1016/j.carbon.2011.06.099](https://doi.org/10.1016/j.carbon.2011.06.099).

REFERENCES

- [1] Wen ZH, Li JH. Hierarchically structured carbon nanocomposites as electrode materials for electrochemical energy storage, conversion and biosensor systems. *J. Mater. Chem.* 2009;19:8707–13.
- [2] Guo YG, Hu JS, Wan LJ. Nanostructured materials for electrochemical energy conversion and storage devices. *Adv. Mater.* 2008;20:2878–87.
- [3] Thavasi V, Singh G, Ramakrishna S. Electrospun nanofibers in energy and environmental. *Energy Environ. Sci.* 2008;1:205–21.
- [4] Girishkumar G, Hall TD, Vinodgopal K, Kamat PV. Single wall carbon nanotube supports for portable direct methanol fuel cells. *J. Phys. Chem. B* 2006;110:107–14.
- [5] Mu YY, Liang H, Hu JS, Jiang L, Wan LJ. Controllable Pt nanoparticle deposition on carbon nanotubes as an anode catalyst for direct methanol fuel cells. *J. Phys. Chem. B* 2005;109:22212–6.
- [6] Liu HS, Song CJ, Zhang L, Zhang JJ, Wang HJ, Wilkinson DP. A review of anode catalysis in the direct methanol fuel cell. *J. Power Sources* 2006;155:95–110.
- [7] Li HY, Zhang XH, Pang HL, Huang CT, Chen JH. PMo₁₂-functionalized graphene nanosheet-supported PtRu nanocatalysts for methanol electro-oxidation. *J. Solid State Electrochem.* 2010;14:2267–74.
- [8] Seger B, Kamat PV. Electrocatalytically active graphene-platinum nanocomposites. role of 2-D carbon support in PEM fuel cells. *J. Phys. Chem. C* 2009;113:7990–5.
- [9] Liu YC, Qiu XP, Huang YQ, Zhu WT. Mesocarbon microbeads supported Pt-Ru catalysts for electrochemical oxidation of methanol. *J. Power sources* 2002;111:160–4.
- [10] Joo SH, Choi SJ, Oh I, Kwak J, Liu Z, Terasaki O, et al. Ordered nanoporous arrays of carbon supporting high dispersions of platinum nanoparticles. *Nature* 2001;412:169–71.
- [11] Joo SH, Pak C, You DJ, Lee A, Lee HI, Kim JM, et al. Ordered mesoporous carbons (OMC) as supports of electrocatalysts for direct methanol fuel cells (DMFC): effect of carbon precursors of OMC on DMFC performances. *Electrochim. Acta* 2006;52:1618–26.
- [12] Bessel CA, Laubernds K, Rodriguez NM, Baker RTK. Graphite nanofibers as an electrode for fuel cell applications. *J. Phys. Chem. B* 2001;105:1115–8.
- [13] Huang HX, Chen SX, Yuan CE. Platinum nanoparticles supported on activated carbon fiber as catalyst for methanol oxidation. *J. Power Sources* 2008;175:166–74.
- [14] Li WZ, Liang CH, Qiu JS, Zhou WJ, Han HM, Wei ZB, et al. Carbon nanotubes as support for cathode catalyst of a direct methanol fuel cell. *Carbon* 2002;40:791–4.
- [15] Wu G, Xu BQ. Carbon nanotube supported Pt electrodes for methanol oxidation: A comparison between multi- and single-walled carbon nanotubes. *J. Power Sources* 2007;174:148–58.
- [16] Xu JB, Hua KF, Sun GZ, Wang C, Lv XY, Wang YJ. Electrooxidation of methanol on carbon nanotubes

- supported Pt-Fe alloy electrode. *Electrochem. Commun.* 2006;8:982–6.
- [17] Chai GS, Yoon SB, Kim JH, Yu JS. Spherical carbon capsules with hollow macroporous core and mesoporous shell structures as a highly efficient catalyst support in the direct methanol fuel cell. *Chem. Commun.* 2004;23:2766–7.
- [18] Han SJ, Yun YK, Park W, Sung E, Hyeon T. Simple solid-phase synthesis of hollow graphitic nanoparticles and their application to direct methanol fuel electrodes. *Adv. Mater.* 2003;15:1922–5.
- [19] Chai GS, Shin IS, Yu JS. Synthesis of ordered, uniform, macroporous carbons with mesoporous walls templated by aggregates of polystyrene spheres and silica particles for use as catalyst support in direct methanol fuel cells. *Adv. Mater.* 2004;16:2057–61.
- [20] Li MY, Han GY, Yang BS. Fabrication of the catalytic electrodes for methanol oxidation on electrospinning-derived carbon fibrous mats. *Electrochem. Commun.* 2008;10:880–3.
- [21] Zhou YG, Chen JJ, Wang FB, Sheng ZH, Xia XH. A facile approach to the synthesis of highly electroactive Pt nanoparticles on graphene as an anode catalyst for direct methanol fuel cells. *Chem. Commun.* 2010;46:5951–63.
- [22] Stankovich S, Dikin DA, Dommett GHB, Kohlhaas KM, Zimney EJ, Stach EA, et al. Graphene-based composite materials. *Nature* 2006;442:282–6.
- [23] Niyogi S, Bekyarova E, Itkis ME, McWilliams JL, Hamon MA, Haddon RC. Solution properties of graphite and graphene. *J. Am. Chem. Soc.* 2006;128:7720–1.
- [24] Balandin AA, Ghosh S, Bao WZ, Calizo I, Teweldedghan D, Miao FC, et al. Superior thermal conductivity of single-layer graphene. *Nano Lett.* 2008;7:902–7.
- [25] Novoselov KS, Geim AK, Morozov SV, Jiang D, Zhang Y, Dubonos SV, et al. Electric field effect in atomically thin carbon films. *Science* 2004;306:666–9.
- [26] Geim AK, Novoselov KS. The rise of graphene. *Nat. Mater.* 2007;6:183–91.
- [27] Sun ZZ, Yan Z, Yao J, Beitler E, Zhu Y, Tour JM. Growth of graphene from solid carbon sources. *Nature* 2010;468:549–52.
- [28] Ruoff RS. Calling all chemists. *Nat. Nanotechnol.* 2008;3:10–1.
- [29] Park S, Ruoff RS. Chemical methods for the production of graphemes. *Nat. Nanotechnol.* 2009;4:217–24.
- [30] Bai H, Li C, Shi GQ. Functional composite materials based on chemically converted graphene. *Adv. Mater.* 2011;23:1089–115.
- [31] Xu C, Wang X, Zhu JW. Graphene-metal particle nanocomposites. *J. Phys. Chem. C* 2008;112:19841–5.
- [32] Shang NG, Papakonstantinou P, Wang P. Platinum integrated graphene for methanol fuel cells. *J. Phys. Chem. C* 2010;114:15837–41.
- [33] Dong LF, Gari RRS, Li Z, Craig MM, Hou SF. Graphene-supported platinum and platinum–ruthenium nanoparticles with high electrocatalytic activity for methanol and ethanol oxidation. *Carbon* 2010;48:781–7.
- [34] Yoo EJ, Okata T, Akita T, Kohya M, Nakamura J, Honma I. Enhanced electrocatalytic activity of Pt subnanoclusters on graphene nanosheet surface. *Nano Lett.* 2009;9:2255–9.
- [35] Xu YX, Zhao L, Hong BaiH, WJ LiC, Shi GQ. Chemically converted graphene induced molecular flattening of 5, 10, 15, 20-tetrakis (1-methyl-4-pyridinio)porphyrin and its application for optical detection of cadmium(II) ions. *J. Am. Chem. Soc.* 2009;131:13490–7.
- [36] Han GY, Yuan JY, Shi GQ, Wei F. Electrodeposition of polypyrrole/multiwalled carbon nanotube composite films. *Thin Solid Films.* 2005;474:64–9.
- [37] Kudin KN, Ozbas B, Schniepp HC, Homme RKP, Aksay IA, Car R. Raman spectra of graphite oxide and functionalized graphene sheets. *Nano Lett.* 2008;8:36–41.
- [38] Gao XF, Jang J, Nagase S. Hydrazine and thermal reduction of graphene oxide: reaction mechanisms, product structures, and reaction design. *J. Phys. Chem. C* 2010;114:832–42.
- [39] Pozio A, Francesco MD, Cemmi A, Cardellini F, Giorgi L. Comparison of high surface Pt/C catalysts by cyclic voltammetry. *J. Power Sources* 2002;105:13–9.
- [40] Rhee CK, Kim BJ, Ham C, Kim YJ, Song K, Kwon K. Size effect of Pt nanoparticle on catalytic activity in oxidation of methanol and formic acid: comparison to Pt(1 1 1), Pt(1 0 0), and polycrystalline Pt electrodes. *Langmuir* 2009;25:7140–7.
- [41] Yang SH, Chen CY, Wang WJ. An impedance study of an operating direct methanol fuel cell. *J. Power Sources.* 2010;195:2319–30.
- [42] Zhou M, Zhang A, Dai ZX, Feng YP, Zhang C. Strain-enhanced stabilization and catalytic activity of metal nanoclusters on graphene. *J. Phys. Chem. C* 2010;114:16541–6.